NATIONAL RADIO ASTRONOMY OBSERVATORY
Charlottesville, VA

ELECTRONICS DIVISION INTERNAL REPORT NO. 320

ANALYSIS OF A SINGLE-CONVERSION, ANALOG/DIGITAL SIDEBAND-SEPARATING MIXER PROTOTYPE

J. R. Fisher & M. A. Morgan

June 16, 2008

Analysis of a Single-Conversion, Analog/Digital Sideband-Separating Mixer Prototype National Radio Astronomy Observatory Electronics Division Internal Report No. 320

J. R. Fisher & M. A. Morgan

June 16, 2008

Abstract

As part of an initiative to reduce the size, weight, and complexity of radio astronomy receivers and to place the conversion from analog to digital signals as close to the telescope feed as possible, a prototype single-conversion, sideband-separating mixer receiver with a tunable local oscillator (LO) between 5 and 9 GHz has been built and tested. After straightforward gain and phase calibration in digital signal processing, unwanted sideband suppression better than 50 dB is achieved throughout an IF band of ±27 MHz (limited by the sampling speed of the available 14-bit digitizer) and over the full tuning range of the LO. No special phase matching in the analog electronics is required. Calibration vectors can be parameterized in a way that avoids the need for a full two-dimensional (LO and intermediate frequency) measurement matrix. Quantization errors introduced by the digitizer do not degrade sensitivity and sideband suppression as long as the random noise rms voltage is at least 5 sample intervals. The spurious response from the first LO harmonic is about 30 dB down from the fundamental so a switchable low-pass filter at the signal input may be required for operation of the mixer over an LO tuning range greater than about a 1.8:1.

1 Introduction

There are a number of compelling reasons for wanting to reduce the complexity of radio astronomy receivers: lower cost, size, and power consumption for use in arrays (focal plane, aperture, and aperture synthesis), fewer spurious responses from multiple frequency conversions, shorter RF signal path length to minimize the effects of impedance mismatch reflections on spectral baselines, and lower total gain and, hence, better stability. Most of these goals are also served by digitizing the signal as close to the telescope feed as possible so that signal fidelity is not affected by long transmission distances from the feed to the signal processing electronics and recording media in the control building. Early digitization also allows some of the burden of waveguide-to-coax and polarization mode conversions to be moved from RF hardware to digital signal processing and executed with greater precision and stability.

To these ends we are investigating the feasibility of a single-conversion, sideband-separating mixer with a tunable local oscillator (LO) frequency that uses digital signal processing to generate upper and lower sidebands with high sideband separation. The test circuit for this idea is shown in Figure 1. Analog sideband-separating mixers are used extensively at millimeter wavelengths, e.g., [Kerr & Pan.(1996)], but this mixer type has seen limited use at lower frequencies where RFI is a much bigger problem, and sideband isolation requirements are more demanding. Practical phase and amplitude match errors have limited the sideband isolation in analog mixer circuits to about 25 dB with a fixed LO frequency. The mixer described in this report does the baseband phase shift in digital arithmetic, which, after calibration, can compensate for all errors in the analog portion of the mixer circuit to produce very good sideband separation without loss of signal-to-noise performance.

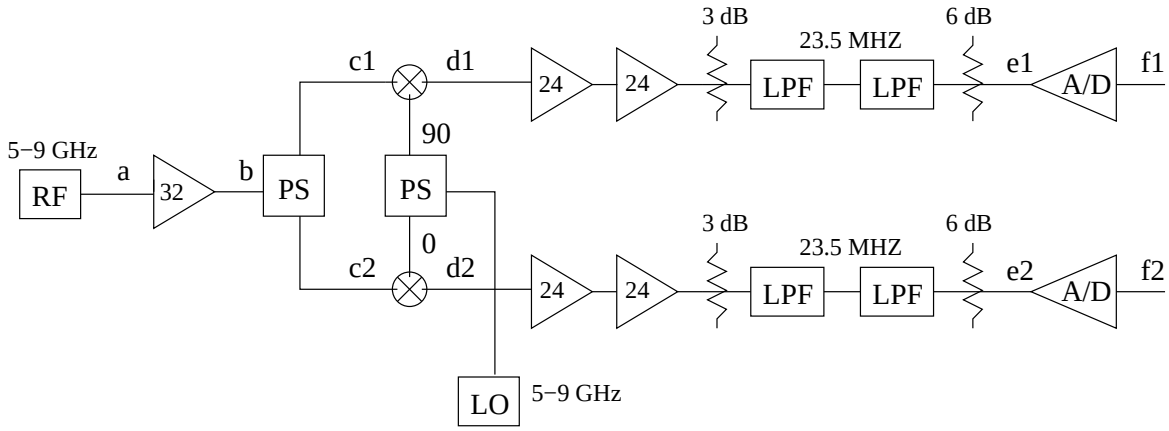

Figure 1: Test circuit for a sideband-separating mixer.

The input of the test circuit is broadband with enough gain to dominate the noise of the mixers and IF amplifiers. The input power splitter has 0^o relative phase outputs, but it could be a 180^o hybrid. The quadrature mixer is implemented with two mixers and a common LO whose output is divided by a 90-degree power splitter. The low-pass filters suppress aliases of the A/D samplers. For this test the sample rate is 60 MS/s, and the 3-dB cutoff frequency of the filter pair is 23.5 MHz. The filters have nominally the same passband and phase delay, but no attempt has been made to match them. All phase and amplitude differences between the two IF channels are intended to be corrected in digital signal processing.

2 Signal Mathematics

Since an RF signal at input point, a, can be decomposed into Fourier frequency components of arbitrarily narrow bandwidth, we can analyze the phase and amplitude history of one of these components in the signal paths as a CW signal without loss of generality. In fact, the first step in digital signal processing will be to do a Fourier transform of a finite-length data sample vector to generate narrow-band samples of all Fourier components in the low-pass filter passband. Each component will be effectively coherent over the length of the data vector.

A CW signal at point, b, can be described in complex notation as

$$Ve^{j\omega t} = V(cos(\omega t) + jsin(\omega t)), \tag{1}$$

where V is the signal peak amplitude, ω is the angular frequency, and t is time. If we take the amplitude and phase of the CW signal in channel 2 as references, then the signal at point, $f1$, in Figure 1 is given by

$$Xe^{j(|\omega-\omega_{LO}|t\pm\phi_{LO}+\phi_f)} = Xe^{j(\omega_{IF}t\pm\phi_{LO}+\phi_f)}, \tag{2}$$

where X is the ratio of amplitudes, V_1/V_2, at points $f1$ and $f2$, ω_{LO} is the LO angular frequency, ϕ_{LO} is the phase difference between the LO signal at the two mixers (nominally 90^o), and ϕ_f is the relative signal phase mismatch between point b and points $f1$ and $f2$ due to differences in cable, amplifier, and filter delays (nominally 0^o). The minus sign on ϕ_{LO} corresponds to a CW signal in the upper mixer sideband, and the plus sign is for the lower sideband.

If, in digital signal processing, we multiply the signal in channel 1 by

$$\frac{1}{X}e^{-j(\phi_f-\phi_{LO}-\pi)} = \frac{-cos(\phi_f-\phi_{LO}) + j\ sin(\phi_f-\phi_{LO})}{X} \tag{3}$$

and add it to the channel 2 signal, the upper sideband signal ($\omega > \omega_{LO}$) will be canceled

$$e^{j\omega_{IF}t} + Xe^{j(\omega_{IF}t-\phi_{LO}+\phi_f)}\frac{1}{X}e^{-j(\phi_f-\phi_{LO}-\pi)} = e^{j\omega_{IF}t} + e^{j(\omega_{IF}t+\pi)} = 0, \tag{4}$$

and the lower sideband signal ($\omega < \omega_{LO}$) will be left.

$$e^{j\omega_{IF}t} + Xe^{j(\omega_{IF}t+\phi_{LO}+\phi_f)}\frac{1}{X}e^{-j(\phi_f-\phi_{LO}-\pi)} = e^{j\omega_{IF}t} + e^{j(\omega_{IF}t+2\phi_{LO}+\pi)}, \tag{5}$$

If ϕ_{LO} is not exactly 90^o, there will be some gain loss in the lower sideband because its signal through the two channels will not add exactly in phase.

Similarly, the lower sideband can be canceled by multiplying the signal in channel 1 by

$$\frac{1}{X}e^{-j(\phi_f+\phi_{LO}-\pi)} = \frac{-cos(\phi_f+\phi_{LO}) + j\ sin(\phi_f+\phi_{LO})}{X} \tag{6}$$

and adding it to the channel 2 signal

$$e^{j\omega_{IF}t} + Xe^{j(\omega_{IF}t+\phi_{LO}+\phi_f)}\frac{1}{X}e^{-j(\phi_f+\phi_{LO}-\pi)} = e^{j\omega_{IF}t} + e^{j(\omega_{IF}t+\pi)} = 0, \tag{7}$$

and the upper sideband is retained.

$$e^{j\omega_{IF}t} + Xe^{j(\omega_{IF}t-\phi_{LO}+\phi_f)}\frac{1}{X}e^{-j(\phi_f+\phi_{LO}-\pi)} = e^{j\omega_{IF}t} + e^{j(\omega_{IF}t-2\phi_{LO}+\pi)}, \tag{8}$$

The calibration task, then, is to determine the gain ratio, X, and the phase terms, $(\phi_f - \phi_{LO})$ and $(\phi_f + \phi_{LO})$, for all frequencies in the IF passband. The gain ratio computation is straightforward. It is just the square root of the quotient of the time-averaged CW signal powers in the two channels.

$$X = \sqrt{\frac{\langle V_1 e^{j\omega t} V_1 e^{-j\omega t}\rangle}{\langle V_2 e^{j\omega t} V_2 e^{-j\omega t}\rangle}} \tag{9}$$

The phase term, $(\phi_f \pm \phi_{LO})$, can be determined from the cross-product of V_1 and V_2. We have defined V_1 and V_2 as

$$V_1 = Xe^{j(\omega_{IF}t+\phi_f\pm\phi_{LO})} \tag{10}$$

and

$$V_2 = e^{j\omega_{IF}t} \tag{11}$$

so

$$V_1 V_2^* = Xe^{j(\phi_f\pm\phi_{LO})} \tag{12}$$

and

$$\phi_f \pm \phi_{LO} = arctan\Big(\frac{Im\langle V_1 V_2^*\rangle}{Re\langle V_1 V_2^*\rangle}\Big) \tag{13}$$

Since the plus sign corresponds to the lower sideband ($\omega < \omega_{LO}$) and the minus sign to the upper sideband ($\omega > \omega_{LO}$), we can define

$$\phi_{LSB} = \phi_f + \phi_{LO} \tag{14}$$

and

$$\phi_{USB} = \phi_f - \phi_{LO} \tag{15}$$

These two quantities can be measured at one intermediate frequency with a CW signal in the upper sideband ($\omega = \omega_{LO} + \omega_{IF}$) and then in the lower sideband ($\omega = \omega_{LO} - \omega_{IF}$), and, if the phase offset between the channels before the mixers is the same in the two sidebands, the LO phase and delay offsets can be separated with

$$\phi_{LO} = \frac{\phi_{LSB} - \phi_{USB}}{2} \tag{16}$$

$$\phi_f = \frac{\phi_{LSB} + \phi_{USB}}{2}. \tag{17}$$

In general, one cannot expect the pre-mixer phase offset to be constant over a wide frequency range so the separation of LO and signal path phases using Equations 16 and 17 only works for small ω_{IF}.

From Equations 3 and 6 the vector multipliers applied to channel 1 needed to **cancel** the upper and lower sideband, respectively, when added to channel 2 are

$$\frac{1}{X} e^{-j(\phi_{USB} - \pi)} = \frac{-cos(\phi_{USB}) + j\ sin(\phi_{USB})}{X} \tag{18}$$

and

$$\frac{1}{X} e^{-j(\phi_{LSB} - \pi)} = \frac{-cos(\phi_{LSB}) + j\ sin(\phi_{LSB})}{X} \tag{19}$$

For the benefit of the computer code, let's define the following quantities:
the channel 1 complex voltage in one spectral channel

$$A + jB, \tag{20}$$

the channel 2 complex voltage in one spectral channel

$$C + jD, \tag{21}$$

the vector to **pass** the upper sideband and **cancel** the lower sideband

$$R_U + jI_U = \frac{-cos(\phi_{LSB})}{X} + j\frac{sin(\phi_{LSB})}{X}, \tag{22}$$

and the vector to **pass** the lower sideband and **cancel** the upper sideband

$$R_L + jI_L = \frac{-cos(\phi_{USB})}{X} + j\frac{sin(\phi_{USB})}{X}. \tag{23}$$

Then the upper sideband signal voltage, without the time-dependent term, will be

$$V_{USB} = (A + jB)(R_U + jI_U) + C + jD = AR_U - BI_U + C + j(AI_U + BR_U + D), \tag{24}$$

and the lower sideband signal voltage will be

$$V_{LSB} = (A + jB)(R_L + jI_L) + C + jD = AR_L - BI_L + C + j(AI_L + BR_L + D), \tag{25}$$

All of the terms in the equations above are frequency dependent and must be calibrated accordingly. The powers at a given frequency in the two sidebands are then

$$P_{USB} = (AR_U - BI_U + C)^2 + (AI_U + BR_U + D)^2 \tag{26}$$

and

$$P_{LSB} = (AR_L - BI_L + C)^2 + (AI_L + BR_L + D)^2 \tag{27}$$

3 Test Setup

A photograph of the test setup is shown in Figure 2. It follows the block diagram shown in Figure 1, with an in-phase splitter on the RF port, and a quadrature hybrid on the LO port. The input signal frequency range is 4-10 GHz, limited at the high end by the splitter, and the LO range is 4-12 GHz. The IF bandwidth is limited by the available sampler card to about 30 MHz.

The RF amplifier is a surplus part borrowed from the ALMA Band 6 program, and has about 32 dB of gain and a noise temperature of 80-120 K across the 4-12 GHz band, as shown in Figure 3. The LO hybrid, also with a 4-12 GHz operating range, is from Mac Technology, model C7256, and has a specified

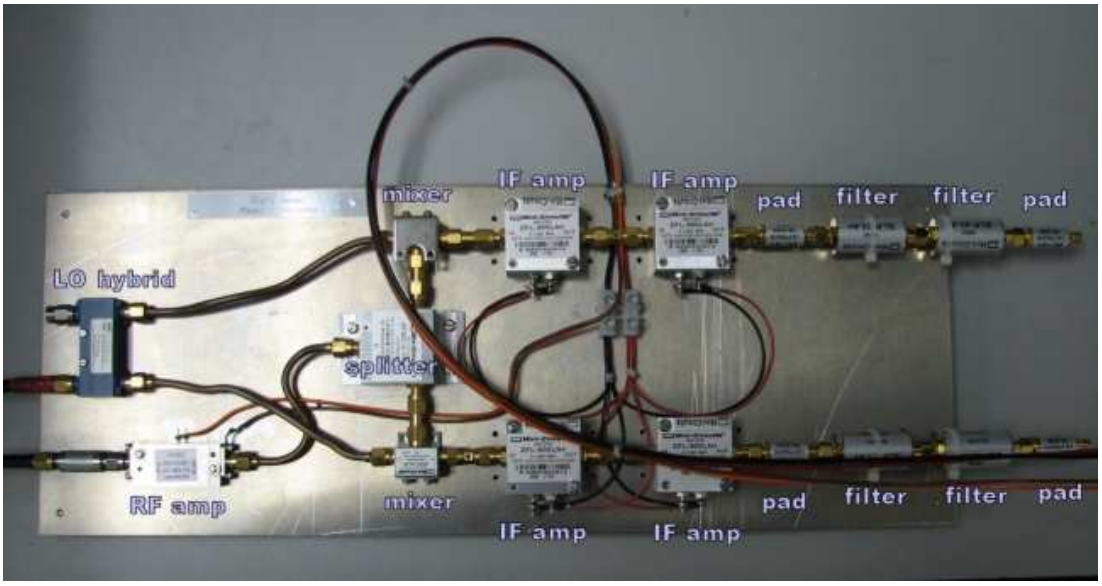

Figure 2: Photograph of the experimental digital image rejection receiver.

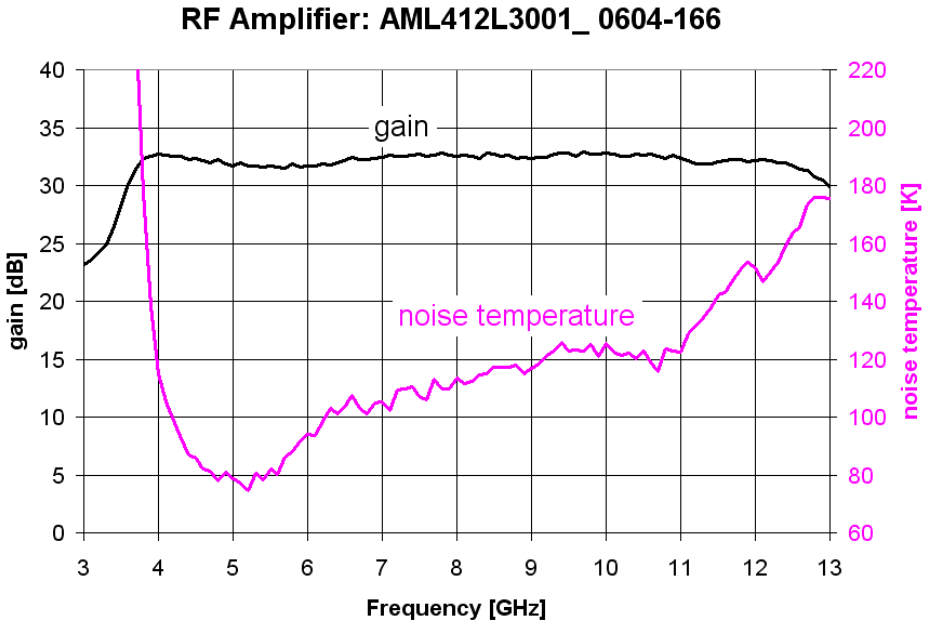

Figure 3: Measured gain and noise temperature data for the RF amplifier.

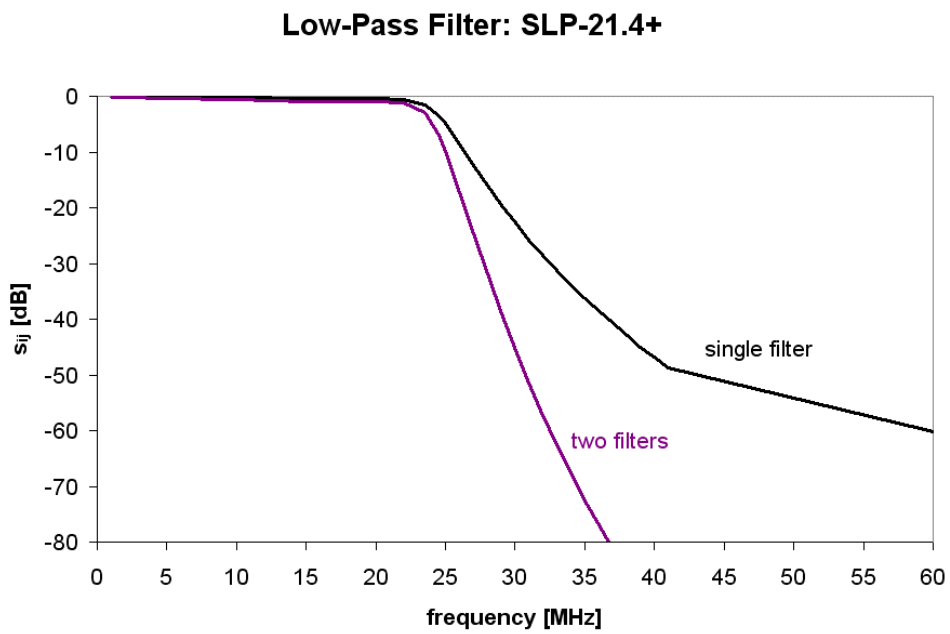

Figure 4: Typical small-signal performance of the low-pass filters.

gain imbalance of about 0.4 dB. The remaining splitter, mixers, amplifiers, pads, and filters, were all purchased off-the-shelf from Mini-Circuits. The filters were selected to avoid aliasing when sampled at a rate of 60 Ms/s. Their passband is shown in Figure 4. Jointly, they have a 3 dB cutoff frequency of about 23.5 MHz. The worst-case aliasing occurs at 30 + (30 - 23.5) = 36.5 MHz, for which the rejection is approximately 80 dB.

The net gain of the test receiver is about 70 dB from the RF input to either IF output. Although similar parts were used in each IF path, no special effort was made to match their complex gains. The semi-rigid coax cables connecting the LO hybrid to the two mixers were approximately the same length, but again no extra care was taken to match them in phase. The RF and LO inputs were generated by Agilent 83640A and 8340B Synthesizers, respectively. The RF synthesizer was set to a power level of -60 dBm for these measurements, with an external 30 dB pad for a net RF CW power of -90 dBm. The LO synthesizer was set to provide +14 dBm to the test set, or approximately +10 dBm for each mixer.

The analog-to-digital conversion was done with a dual-channel, 14-bit, simultaneous sampling ADLink Technologies Model PCI-9820 PC card running at 60 megasamples per second (MS/s) with ±1 Volt full-scale. Data bursts were recorded in memory on the A/D card for 0.3 seconds and then transferred to PC hard disk storage at a rate limited by the PCI bus. All data reported here are based on this 0.3-second integration period, which was sufficient for test purposes.

4 Data Processing

The first step in all data processing was to do a real-to-complex discrete Fourier transform on simultaneously sampled, 4096-point raw data windows from the two A/D's using a cosine window taper function to produce good channel-to-channel isolation in the resulting 2049-point spectra. Adjacent time windows were overlapped by 50% to avoid significant loss of sensitivity. From these two complex spectra four real spectra products were produced and time-averaged for the 0.3-second data block: channel 1 squared, channel 2 squared, and the real and imaginary parts of channel 1 times channel 2, as shown on the right hand side of Equations 9 and 13. Examples of these four baseband spectra are shown in

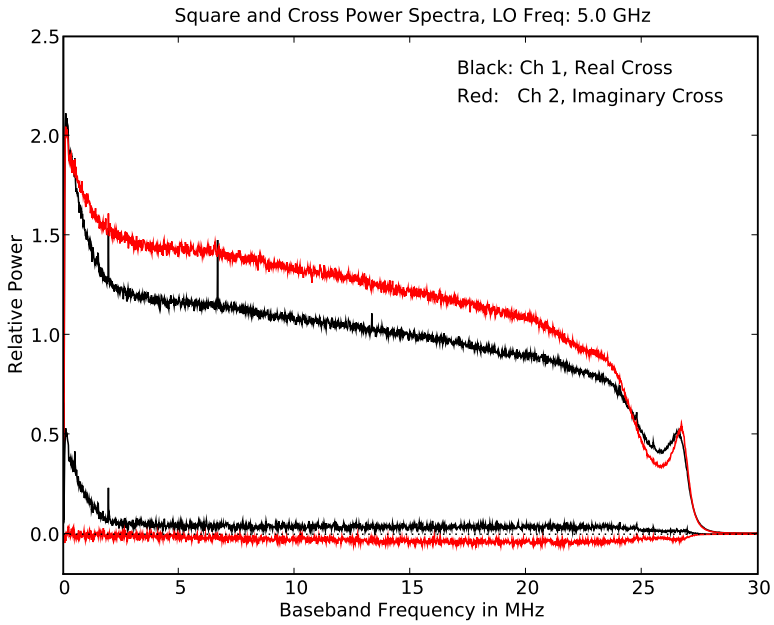

Figure 5: Baseband square and cross-product noise power spectra with an LO frequency of 5000 MHz.

Figure 5. In the absence of correlated noise the cross product spectra would be zero amplitude so the non-zero levels must be due to noise from the amplifier before the signal path power splitter. There are several weak, narrowband signals near 2, 7, and 26 MHz that leaked into our system after the mixers from the lab environment, but these did not interfere with our measurements.

To calibrate the phase offsets and amplitude ratios in both sidebands and across the full baseband frequency range a CW signal with a power roughly equal to the total passband noise power was injected at the receiver input, as shown in Figure 1, and stepped in frequency across the full lower and upper sideband range. Since this signal appears in only one or two channels of the output spectrum, its signal to noise ratio in 0.3 seconds of data is quite high as can be seen in the logarithmic amplitude plot of Figure 6.

The amplitude ratio and phase quantities on the left side of Equations 9, 14, and 15 were measured at a set of RF frequencies across the mixer input frequency range at one LO setting by stepping the input CW signal by 0.5 MHz between each 0.3-second data burst. The quantities, X and ϕ_{USB} or ϕ_{LSB} were computed from the spectral channel containing the largest amount of CW power. The results are shown in Figures 7 and 8. Comparison of amplitude ratios in the two sidebands at the same intermediate frequencies (IF) shows close but not exact match, possibly due to different effects of impedance mismatches on the mixer ports for the two sidebands. This difference may be important for maximum sideband isolation.

The phase offsets shown in Figure 8 are approximately $\pm 90^o$, as expected, but phase error in the LO quadrature power splitter and phase mismatches between the two signal paths (mainly in the low-pass filters) are evident. The LO and signal path phase errors may be separated according to Equations 16 and 17 and are plotted in Figure 9. The LO phase component is constant, as expected for a fixed LO frequency, at $91.8^o \pm 0.1^o$ for all CW signal frequency pairs (LSB and USB for a given IF).

The final step in data processing was to use the phase data shown in Figures 7 and 8 to separate the two sidebands using Equations 20 through 27 point by frequency point in the baseband spectrum for each pair of 4096-sample blocks of raw data. The P_{LSB} and P_{USB} values for each frequency point were time averaged over the 0.3-second data interval to produce integrated upper and lower sideband spectra

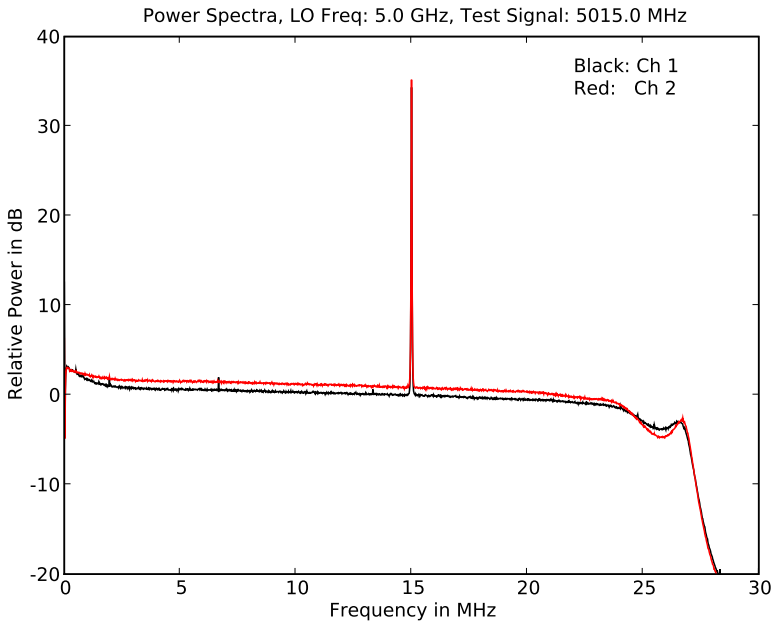

Figure 6: Baseband noise power plus CW test signal spectra with an LO frequency of 5000 MHz and a test signal frequency of 5015 MHz. Note the logarithmic vertical scale.

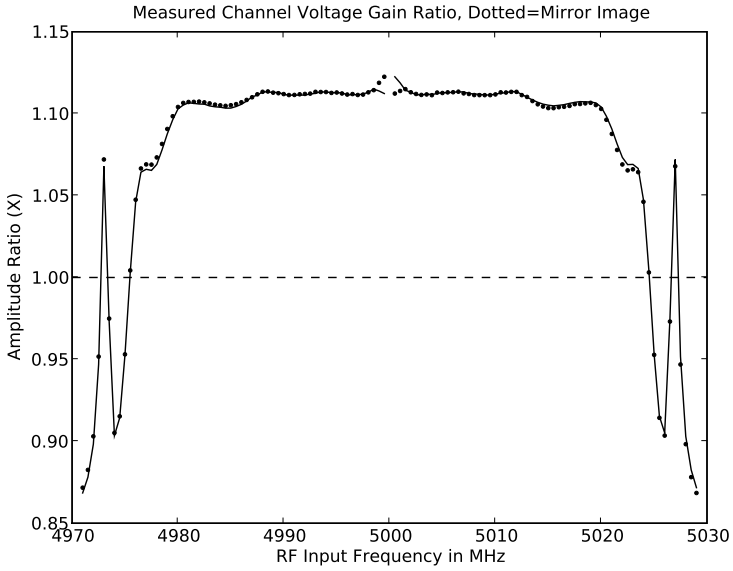

Figure 7: Measured amplitude ratio (X in Equation 9) of the test signal measured at the inputs to the two A/D converters as a function of input test frequency at 0.5 MHz intervals. The solid lines connect the measurements plotted in the correct sideband, and the dots are the the opposite sideband values mirrored across the LO frequency.

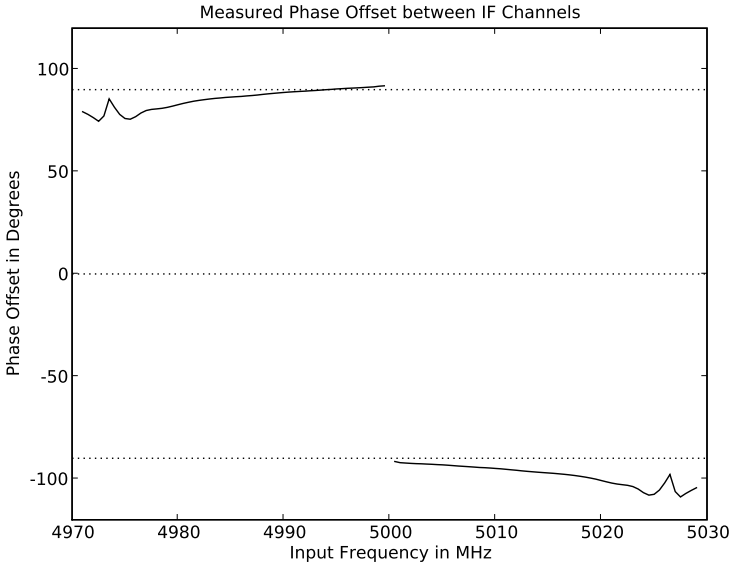

Figure 8: Measured phase offset (ϕ_{USB} and ϕ_{LSB} in Equations 14 and 15) of the test signal measured at the inputs to the two A/D converters as a function of input test frequency at 0.5 MHz intervals. The LO frequency was 5000 MHz.

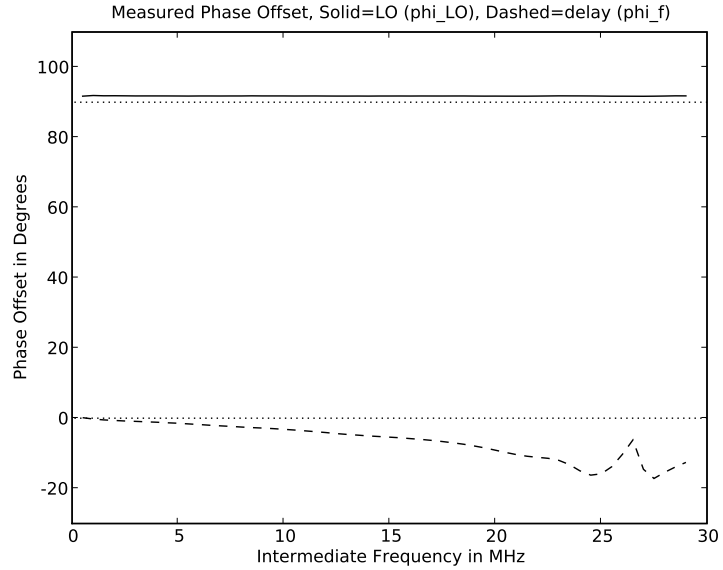

Figure 9: Measured phase offset components for the LO (ϕ_{LO}, solid curve) and RF/IF (ϕ_f, dashed line) signal paths as a function of the intermediate frequency of the CW test signal as derived from the data in Figure 8 using Equations 16 and 17. The LO frequency was 5000 MHz.

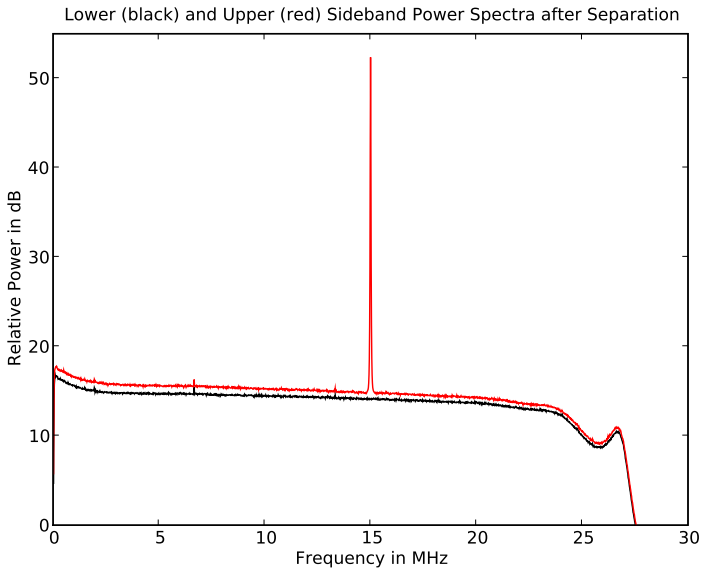

Figure 10: Upper and lower sideband spectra after sideband separation using Equations 26 and 27 and the phase coefficients plotted in Figures 7 and 8. The lower sideband spectrum is displaced downward by 1 dB for clarity. The LO frequency was 5000 MHz and a CW signal was present at the mixer input at 5015 MHz. Calibration and test data were recorded about two hours apart.

that were inspected for sideband separation. Since the phase-offset and amplitude-ratio coefficients were measured for a limited number of CW test signal frequencies, the coefficients for a given frequency point in the spectra were derived by interpolating the real and imaginary coefficient components between the nearest two test frequency coefficients. Figure 10 shows the upper and lower sideband spectra with a CW input signal at a baseband frequency of 15 MHz. The data shown in Figure 10 were recorded about two hours after the calibration data were taken. No signal is apparent in the wrong sideband.

5 Test Results

5.1 Sideband Separation

Figure 11 shows the measured sideband suppression at 1 MHz intervals over the full range of the mixer response with a LO frequency of 5000 MHz. Sideband suppression is defined as the ratio of CW signal power at the same intermediate frequency measured in the two sidebands with the amplifier noise power subtracted. Amplifier noise was measured as the average of two power values that were four frequency points above and below the CW signal frequency. In the absence of a measurable signal, about half of the CW power values were below the baseline due to random noise, and these are shown as upper limits in Figure 11. Except for a couple of points in the upper sideband above the cutoff of the low-pass filter, all points in this figure are consistent with random noise so the suppression may be somewhat better than the conservative upper limit of -55 dB. Better sensitivity to the unwanted sideband CW signal could have been obtained with longer FFT lengths (higher frequency resolution), but the -55 dB limit seemed sufficient for these tests.

The calibration data for the coefficients used to separate sidebands in the data used for Figure 11 were taken at CW frequencies 0.5 MHz apart beginning at 4871.0 MHz, and the test signals were recorded at 1.0 MHz intervals beginning at 4871.0 MHz. Hence, no frequency interpolation of the coefficients was required at the test frequencies. To test the interpolation accuracy, the same test data were used with

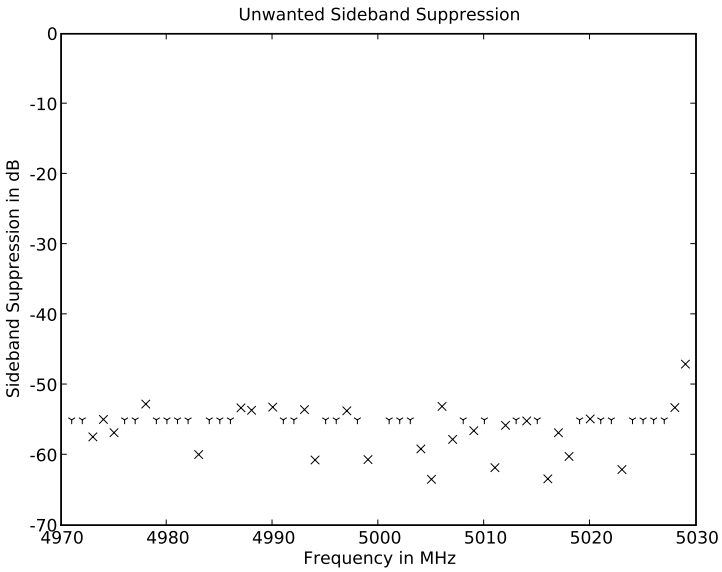

Figure 11: Unwanted sideband suppression of the full mixer frequency range at an LO frequency of 5000 MHz. Spectrum values that were below the surrounding baseline due to random noise are marked as upper limits at -55 dB with a downward pointing tripod symbol. Calibration and test data were recorded about two hours apart.

half of the same coefficients only at half-MHz frequencies, i.e., 4871.5, 4872.5, etc. The results are shown in Figure 12. The interpolation works well for intermediate frequencies below about 23 MHz, Closer to the extremes of the mixer frequency range the sideband suppression suffers from poor coefficient interpolation. Figures 7 and 8 clearly show that the amplitude ratios and phase offsets between the two IF channels are undersampled in frequency near the band edges. This is something to keep in mind when designing the mixer circuit (more gradual band edge roll-offs) or performing the calibration procedure (denser sampling near filter roll-offs). A more sophisticated interpolation algorithm than the linear one used here may also help, but interpolation can be unstable in sparse data, particularly near the ends of the data range.

Equations 28 and 29 give the the sideband suppression expected from modest coefficient errors in phase offset or amplitude ratio, respectively,

$$S(dB) = 20log_{10}(\pi\phi_{err}/180) - 6.02 \tag{28}$$

$$S(dB) = 20log_{10}(X_{err} - 1) - 6.02 \tag{29}$$

where the phase error, ϕ_{err} is in degrees, and the amplitude error is the ratio of the true amplitude ratio (see Equation 9) and the assumed value. The extra 6.02 dB is due to the fact that the error signal is in only one of the two sampled signals. Hence, a 1^o phase error will limit the sideband suppression to -41.2 dB or a 1.16% (0.1 dB) amplitude error will limit the suppression to -44.7 dB. Figure 13 shows the sideband suppression for the data and conditions used in Figure 11 but with a phase or amplitude error of 1^o or 0.1 dB, respectively, applied to the coefficients. The measured sideband suppressions agree well with those computed from Equations 28 and 29.

5.2 Calibration

In principle, the mixer phase coefficients need to be calibrated for all LO frequency settings and all RF input frequencies within the IF passband of each LO frequency, which is a daunting two dimensional

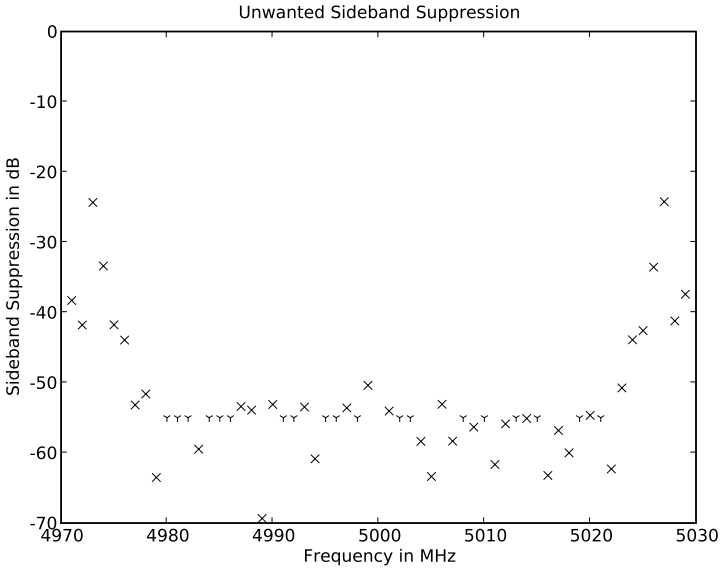

Figure 12: Unwanted sideband suppression of the full mixer frequency range at an LO frequency of 5000 MHz using CW test frequencies at even MHz frequencies (4871.0, 4872.0,...MHz) and coefficients at half-MHz frequencies (4871.5, 4872.5,...MHz) and the sames data as Figure 11. Spectrum values that were below the surrounding baseline due to random noise are marked as upper limits at -55 dB with a downward pointing tripod symbol.

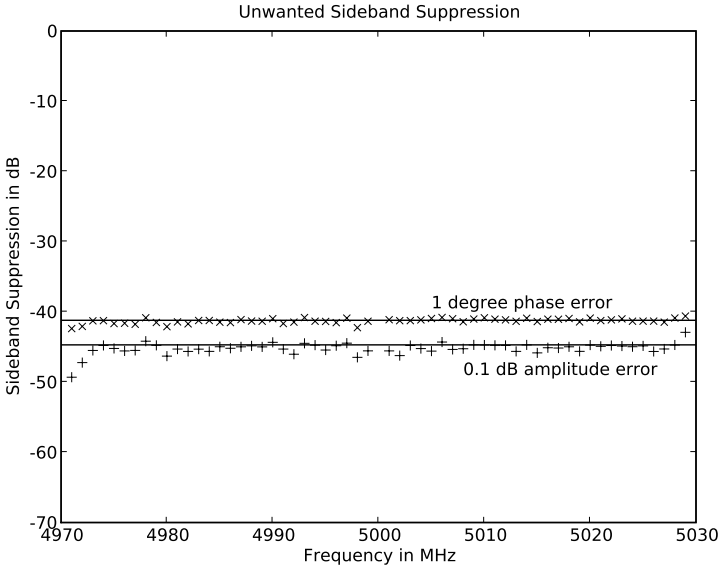

Figure 13: Unwanted sideband suppression for the same data used in Figure 11 but with a phase error of 1^o (x) or an amplitude error of 0.1 db (+) applied to the calibration coefficients. The horizontal lines through the data points are the predicted levels from Equations 28 and 29.

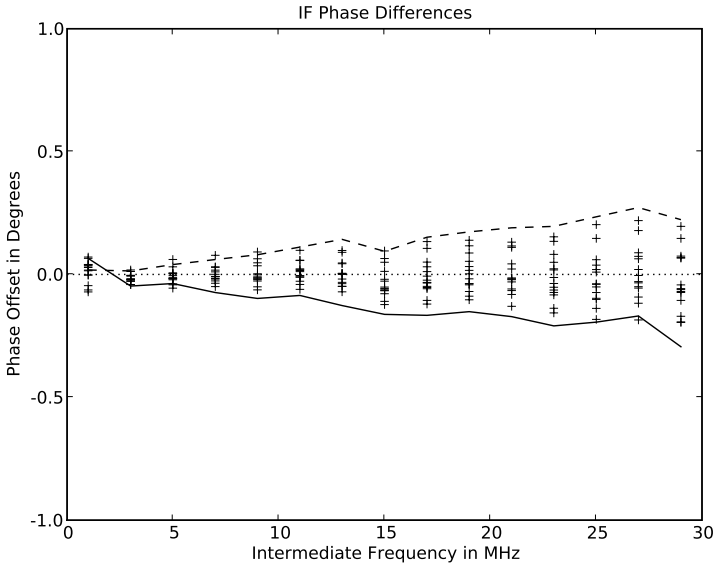

Figure 14: Differences in signal path phases, ϕ_f, measured at an LO frequency of 7000 MHz from those measured at all other LO frequencies between 5000 and 9000 MHz. The solid line connects the points measured at 5000 MHZ, and the dashed line runs through the 5200 MHz points.

calibration task unless the LO phase and signal path phase offsets can be largely decoupled as is suggested by Figure 9. To test the degree to which the LO and signal path phases can be independently calibrated, CW test signals were measured a 2 MHz intervals over the full upper and lower sideband frequency range, $f_{LO} \pm 30MHz$, for LO frequencies from 5000 to 6000 MHz at 100 MHz intervals and from 6000 to 9000 MHz at 500 MHz intervals. The signal path phase offset, ϕ_f, as a function of intermediate frequency measured at an LO frequency of 7000 MHz is chosen as a standard and the phase differences from this curve measured at other LO frequencies plotted in Figure 14. From this figure we can see that the maximum error in the signal path phase caused by measuring it only at the center of the LO tuning range is less than 0.3 degrees. From Equation 28 this corresponds to a minimum sideband suppression of 51.6 dB. The phase error is less at the low end of the IF passband, and the errors are systematically low or high for a given LO frequency as shown by the solid and dashed curves in Figure 14. This systematic error varies fairly rapidly and not monotonically with LO frequency so it might be a bit tedious to parameterize for better accuracy, but it would be less time-consuming than measuring a full two-dimensional set of coefficients.

Figure 15 shows the LO phase offset, ϕ_{LO}, measured with CW test frequency offsets from the LO from ± 1 to ± 29 MHz at 2 MHz intervals and at LO frequencies from 5000 to 9000 MHz as described in the previous paragraph. All 15 CW test frequency pair phase measurements at a given LO frequency agree well enough that their individual symbols in Figure 15 are nearly indistinguishable. However, the variation with LO frequency is substantial, and this variation is too sparsely sampled with the measurement intervals chosen for accurate interpolation, even between 5000 and 6000 MHz, where the spacing is 100 MHz. Since no special care was taken to match cable lengths between the quadrature LO power splitter and the mixers, some phase deviation from 90^o is expected. The trend of the measured LO phase with frequency is roughly the same as that measured with a vector network analyzer (solid curve in Figure 15), but they do not agree in detail. This may be due to differences in the mixers and reflections from the various component ports. The most significant point to be made here is that, with accurate calibration, the unwanted sideband suppression is not seriously degraded by the LO phase offset of 60^o instead of the ideal 90^o at 9000 MHz, as is shown in Figure 16.

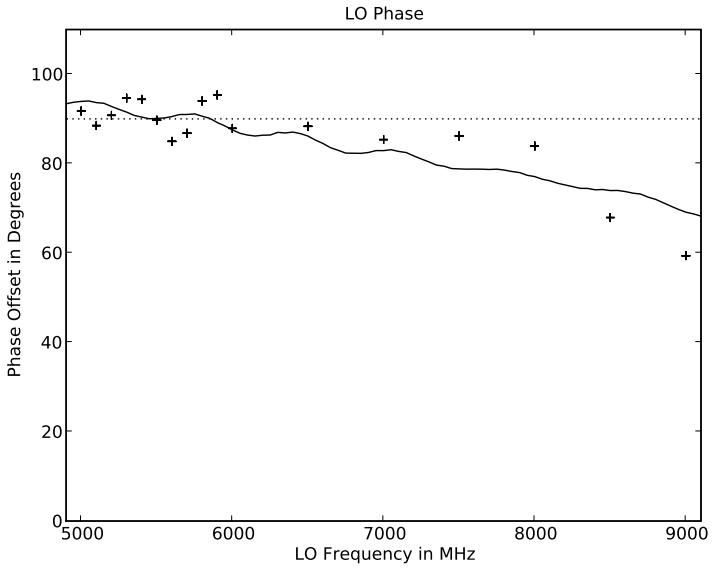

Figure 15: LO phase offsets, ϕ_{LO}, measured with with CW test frequency offsets from the LO from ± 1 to ± 29 MHz at 2 MHz intervals and at LO frequencies from 5000 to 9000 MHz. The solid curve is the phase difference between the mixer ends of the cables from the LO quadrature hybrid measured with a vector network analyzer.

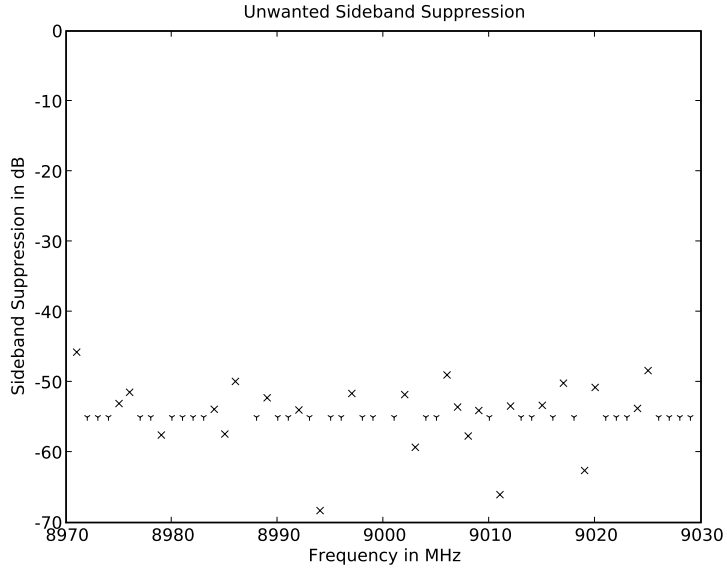

Figure 16: Unwanted sideband suppression of the full mixer frequency range at an LO frequency of 9000 MHz. Spectrum values that were below the surrounding baseline due to random noise are marked as upper limits at -55 dB with a downward pointing tripod symbol. Calibration and test data were recorded about one and a half hours apart.

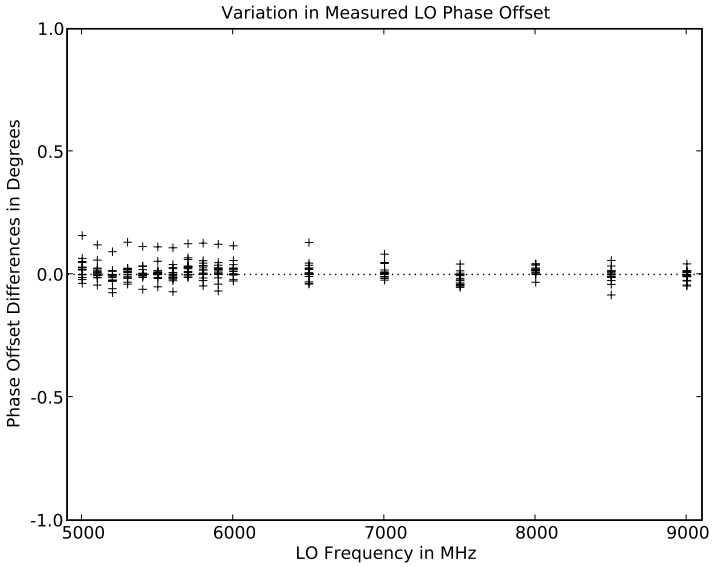

Figure 17: Differences in LO phase offsets, ϕ_{LO}, from a "standard" curve measured with with a CW test signal offset of ±15 MHz from the LO frequency. The symbol locations correspond to measurements with CW test frequency offsets from the LO of ±1, ±3, ... ±13, ±17, ... ±29 MHz.

To test the accuracy of measuring LO phase offset with only one pair of CW test signal frequencies for each LO frequency, the difference between ϕ_{LO} values measured with an offset of ±15 MHz and values measured with CW test frequency offsets between ±1 and ±29 MHz at 2 MHz intervals are plotted in Figure 17. The differences are all less than 0.13 degrees, which corresponds to a minimum sideband suppression of 58.9 dB from Equation 28. The largest phase difference from nominal was measured at a CW offset of ±1 MHz from the LO frequency. Otherwise, the phase differences are consistent with the measurement errors associated with the signal-to-noise ratio of the CW test signal.

5.3 Quantization Effects

The analog-to-digital conversion process introduces quantization errors in the instantaneous RF signal amplitude measurements. On a pure sine wave these quantization errors generate harmonics, and when more than one sine wave is present intermodulation products are produced. When random noise is added to the sine waves the harmonics and intermodulation products are largely converted into tolerable white noise, [Fisher (1999)], but narrowband power is still lost to these products. The number of bits in the A/D converter determines its size and power consumption at a given sampling speed so the number of bits required is an important design parameter for the sideband separating mixer. The data taken for these experiments were examined for quantization effects by successively masking of low-order bits in the A/D output words.

In the absence of a CW test signal at the mixer input, the root-mean-square (rms) noise level at the A/D inputs was about 25 sample intervals, which is equivalent to $Log_2(25) = 4.6$ bits. Figure 18 shows the distribution of sampled data values in two 0.3-second data sets from one sampler, with and without a CW test signal. Figure 19 shows the noise-only distribution of samples with the four least significant bits set to zero.

A useful measure of signal lost to harmonics is the ratio of measured CW power in the spectrum to the rms noise value computed for a quiet portion of the same spectrum with only white noise. Figure 20 shows the relative CW signal power, rms value of the spectral noise, baseline, and the ratio of the two

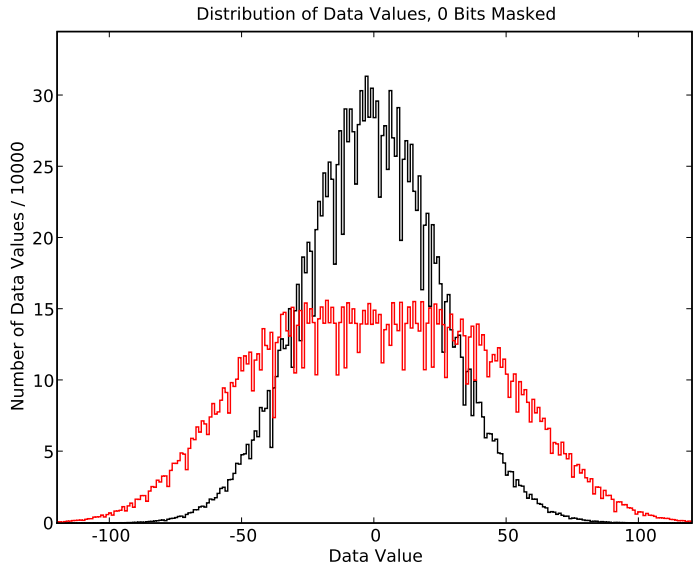

Figure 18: Distribution of sampled data values in two 0.3-second data sets from one sampler, with (broader distribution) and without a CW test signal. The large deviations from smooth distributions are due to uneven A/D sample level spacing, which is characteristic of many high-speed A/D converters.

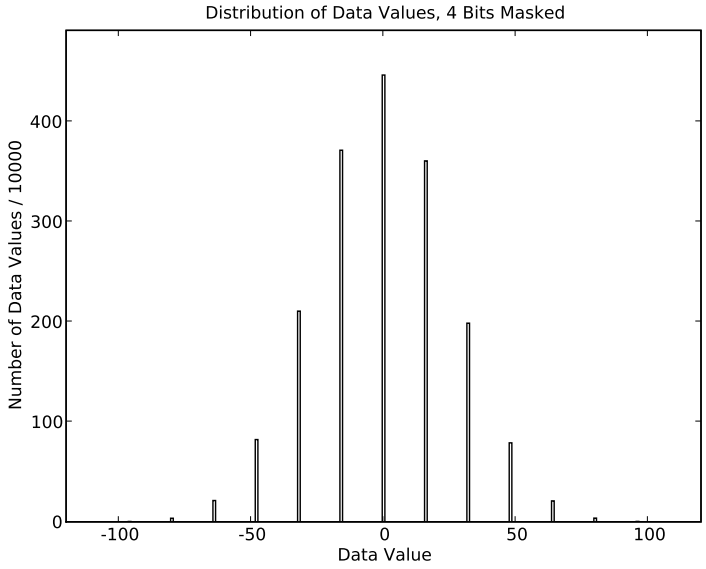

Figure 19: Distribution of sampled noise-only data values in a 0.3-second data set from one sampler with four low-order bits masked (set to zero).

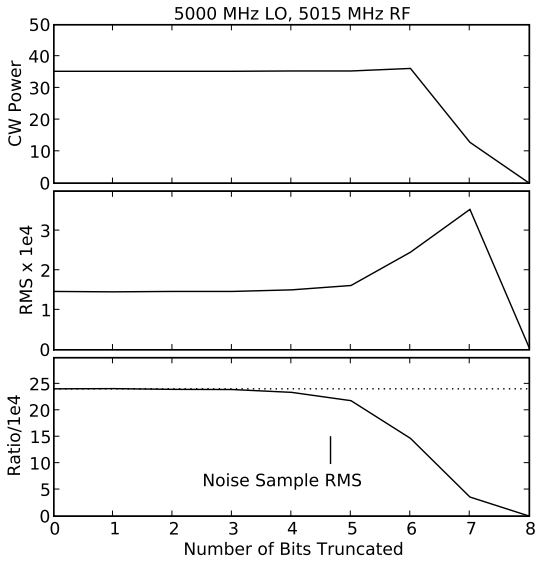

Figure 20: Relative CW signal power, rms value of the spectral noise baseline, and the ratio of the two as a function of the number of least significant bits masked off for the same data taken with an LO frequency of 5000 MHz and CW test signal frequency of 5015 MHz.

as a function of the number of least significant bits set to zero. The CW signal was at an intermediate frequency of 15 MHz, and the section of spectrum used in computing the noise rms ran from 15.3 to 18.0 MHz. A linear baseline was fit by least squares to this piece of spectrum and subtracted to remove the DC power and first derivative of the spectral values as a function of frequency before computing the rms.

Figure 20 indicates that two and possibly three low-order bits can be dropped from the data without substantial loss of narrowband signal power to harmonics. Hence, an rms data sample value of about 5 sample intervals can be used as a rule of thumb for the input level operating point of the A/D with random noise. Masking off low-order bits reduces the error due to uneven sample level spacing so just reducing the signal level may not produce exactly the same results. The curious result that the CW signal power is slightly higher when 5 and 6 bits are masked is probably due to the exact distribution of data values and would vary with small changes in signal level. This is a non-linear range of the A/D converter transfer function for random noise signals that is best avoided for high fidelity, post-sampling signal processing. However, low-order bit masking has very little effect on the accuracy of unwanted sideband suppression. Calibration coefficients generated with data that had 5 bits masked still produced 55 dB or more of sideband suppression.

5.4 Spurious Response from LO Harmonic

An expected spurious response of the sideband-separating mixer is the product of input signals with harmonics of the LO. For example, with an LO frequency of 5000 MHz a signal at 10015 MHz will produce an intermediate frequency of 15 MHz. Measurement of this frequency combination showed the LO harmonic response to be 31 dB below the fundamental response. Further suppression of this spurious response will require a low-pass filter before the mixer. If the mixer tuning range is required to be close to or greater than one octave, then switchable low-pass filters are needed. Since these filters can be placed before the input power splitter they will not affect the mixer phase and amplitude calibration.

6 Future Work

One important aspect of this concept which has not yet been tested is the stability of the calibration with time and temperature. In other words, how often must the digital coefficients be re-calibrated to achieve a given level of sideband-suppression? Is it sufficient to perform a dense calibration of frequency points only once in the lab? Is the calibration repeatable with temperature, such that an empirical model could be developed on the bench? Note that calibration on the telescope can be done fairly simply with a signal injected before the mixer input power splitter so bench calibration is not a prerequisite.

The fact that much of the data presented in this report was taken a couple of hours after the initial calibration was done is evidence that the performance can be quite stable. However, getting realistic numbers for long-term stability will require re-packaging the receiver into a more integrated form with wider IF bandwidth (limited in this report only by the inexpensive sampler), similar to how it would be used on an actual telescope. Another important test is to evaluate the digital sideband-separation receiver in an environment with significant amounts of RFI to see if there are any unexpected artifacts or practical issues. To address these issues, construction of an integrated warm-receiver package targeting the GBT L-Band receiver has been initiated. This package will directly follow the cryogenic portion of the existing receiver, and will process the entire band at once with a single fixed LO.

Since drift in the IF path from the telescope back to the digital electronics will undoubtedly limit the stability and performance of this concept, the problem of integrating the samplers in a compact form with the warm-analog electronics will also be addressed. The obvious technical challenge in this case is isolation of the digital and analog signals. This it is a necessary step in the evolution of the next generation of radio-astronomy receivers.

References

[Kerr & Pan.(1996)] A. R. Kerr and S.-K. Pan, "Design of planar image-separating and balanced SIS mixers," Proceedings of the Seventh International Symposium on Space Terahertz Technology, pp. 207-219, 12-14 Mar 1996. ALMA Memo 151.

[Fisher (1999)] R. Fisher, "Effects of Noise on Sampler Quantization Errors" http://www.cv.nrao.edu/ rfisher/SamplerErr/harmonics.html